RESEARCH ARTICLE

In situ bioprinting for cartilage repair using a parallel manipulator

Hao-Yang Lei[1,2†], You-Rong Chen[1,3,4†], Zi-Bin Liu[2], Yi-Nong Li[2], Bing-Bing Xu[1,3,4]*, Chang-Hui Song[2]*, and Jia-Kuo Yu[1,3,4]*

[1]Department of Sports Medicine, Peking University Third Hospital, Institute of Sports Medicine of Peking University, Beijing, China

[2]School of Mechanical and Automotive Engineering, South China University of Technology, Guangzhou, China

[3]Beijing Key Laboratory of Sports Injuries, Beijing, China

[4]Engineering Research Center of Sports Trauma Treatment Technology and Devices, Ministry of Education, Beijing, China

(This article belongs to the *Special Issue: Light-Based Bioprinted Scaffolds for Tissue Engineering*)

†These authors contributed equally to this work.

*Corresponding authors:
Bing-Bing Xu
(xubingbing@hsc.pku.edu.cn)

Chang-Hui Song
(chsong@scut.edu.cn)
Jia-Kuo Yu (yujiakuo@126.com)

Abstract

Regeneration of large-sized cartilage injury is a challenging endeavor. *In vitro* bioprinting for cartilage repair has several drawbacks, such as the tedious process of material preparation, potential contamination, and the mismatch between implant and defect. This study aimed to investigate the application of *in situ* bioprinting in cartilage repair using a parallel manipulator. In particular, the material extrusion rate and printing speed were adjusted to obtain the suitable forming parameters in a custom-made parallel manipulator. Cell experiments were conducted to determine the biocompatibility. Finally, a rabbit cartilage defect model was used to evaluate the feasibility of *in situ* bioprinting combined with machine vision. The results showed that to achieve optimum printing using the custom-made three-dimensional printer, 400–560 mm/min should be set as the standard printing speed, with an extrusion multiplier of 0.09–0.10. Cartilage defects can be precisely and easily segmented using a bimodal method with a 2% deviation error. *In vitro* experiments revealed that the utilized materials are highly biocompatible. Furthermore, according to the results from *in vivo* experiments, *in situ* bioprinting lends itself useful in the repair of cartilage defects. The overall results confirmed the feasibility of applying a parallel manipulator in *in situ* bioprinting for cartilage repair. Additional optimizations of the proposed approach are warranted prior to translation into clinical applications in the future.

Keywords: *In situ* bioprinting; Cartilage repair; Tissue engineering

1. Introduction

Articular cartilage defects are usually caused by external trauma, joint injury, or other diseases.[1] However, the lack of vasculature, nerves, and lymph in the cartilage restricts its regeneration.[2] A degraded cartilage without prompt and effective treatment can adversely affect the subchondral bone, which, in the worst case, may lead to a situation necessitating knee replacement.[3] Thus, cartilage injury must be treated in the shortest possible time. Conventional treatment methods, such as osteochondral transplantation, bone marrow

stimulation, or autologous chondrocyte transplantation, are generally utilized to treat cartilage injuries, but certain risks exist during or after using these therapies.[4]

Given the continuous development of the field of tissue engineering, new therapeutic ideas for cartilage repair have been constantly generated. As an essential tissue engineering component, the scaffold acts as a temporary filling volume that provides a frame for cell adhesion, migration, and proliferation. Thus, the therapeutic efficacy of tissue engineering is affected by the material and morphology of the scaffold. Usually, porous scaffolds are fabricated by free-drying, thermally-induced phase separation, or electrospinning.[5] Nevertheless, these methods fail to precisely control the shape and distribution of pores. The development of bioprinting has made it possible to fabricate scaffolds with controllable morphology. At present, bioprinting is most commonly used to print a scaffold, using the extracellular matrix (ECM)[6,7] or components that mimic the chondroid tissue.[8,9] Apart from that, there exists a method that uses a sacrificial mold, through which the scaffold is fabricated indirectly.[10,11] However, there are certain limitations in using *in vitro* bioprinting to print cartilage repair scaffolds directly or indirectly. The scaffolds manufactured by the above methods require a complex and cumbersome preparation process prior to implantation. In addition, the steps starting from the printing process (outside) to the implantation are at a potential risk of contamination.[12-14] Furthermore, during surgery, the difficulty associated with fixing the implant constitutes another barrier.[15]

In situ three-dimensional (3D) printing stands as a possible solution to the aforementioned problems commonly seen in non-*in situ* printing. *In situ* bioprinting refers to the direct printing of specific scaffolds on the untreated part.[13] Currently, this technology has been applied to fabricate different tissues, such as skin, bone, and cartilage. For instance, O'Connell *et al.* developed a device called "biopen," through which cell-laden printing can be realized.[16] Hakimi *et al.* invented a handheld skin printer that can *in situ* crosslink the bioink and deposit biomaterials for multilayer skin repair.[17] Chen *et al.* used a manipulator to induce hair follicle-inclusive skin regeneration.[18] Moncal *et al.* pioneered an *in situ* bioprinting system featuring a multi-arm design, aiming to reconstruct tissues within craniomaxillofacial defects.[19,20] In addition, they leveraged this bioprinting system to discern the contrasting effects of *in situ* and *ex situ* delivery systems on calvarial defects.[21] In other examples, Di Bella *et al.* used a biopen with a multi-channel to repair cartilage defects,[22] and Ma *et al.* utilized a robot arm to extrude hyaluronic acid methacrylate (HAMA) into the defect in order to repair cartilage injury.[23] The above *in situ* bioprinting approaches can be divided into two types, i.e., handheld and robot-assisted. The handheld device can deposit the bioink directly, which is more portable and convenient compared to robot-assisted systems.[13] However, the shape printed via handheld devices is difficult to control.[19] Although the cost of robot-assisted systems is higher, their accuracy surpasses that of handheld ones.[24] The robot-assisted approach enables meticulous control over the deposition of bioink, leading to the *in situ* formation of structured scaffolds.

In robot-assisted *in situ* bioprinting, the key step is to determine the trajectory via the reconstruction of the defect. At present, the application of 3D scanner is a common scene in most studies.[23,25] By comparing the impaired cartilage with the healthy part, the defect can be identified and reconstructed. This comparison method is suitable for pre-surgical planning. Nevertheless, since the primary focus during the surgery is on the damaged cartilage, it is therefore challenging to acquire information about the normal cartilage in healthy regions. Thus, reconstructing the defect through comparison becomes difficult, and a reconstruction method without comparison is necessary. To this end, a segmentation approach needs to be employed, through which a defect can be distinguished from the healthy cartilage. Classical segmentation methods include edge detection,[26,27] region division,[28] graph-based segmentation,[29] clustering,[30] and random walk.[31] The integration of deep learning into these basic segmentation methods has spawned the emergence of more intelligent segmentation techniques.[32]

In view of the existing shortcomings of *in situ* bioprinting, we developed a parallel manipulator capable of photocuring and optimized the printing parameters to ensure that the filament was stable and controllable during printing. Moreover, a camera was used during the reconstruction process of cartilage defects via machine vision. By combining the parallel manipulator and machine vision, *in situ* recognition and repair can be achieved.

2. Materials and methods

2.1. Design of the *in situ* parallel manipulator

A custom-made *in situ* 3D printer with dimensions of 350 mm× 350 mm × 300 mm was developed (Figure 1). The extruder was connected to the sliders with three pairs of rods. By asynchronously controlling the movement of the sliders, the extruder can be moved freely in three dimensions and the workspace of the printer is Ø200 × 90 mm, covering the area of the cartilage requiring repair. The extrusion head comprised a screw rod, a bioink storing cartridge, and a curing light source. The bioink was extruded through the movement of a piston in the cartridge driven by a screw rod. A 405-nm light-emitting diode (LED) was used as the light source and arranged in a ring-
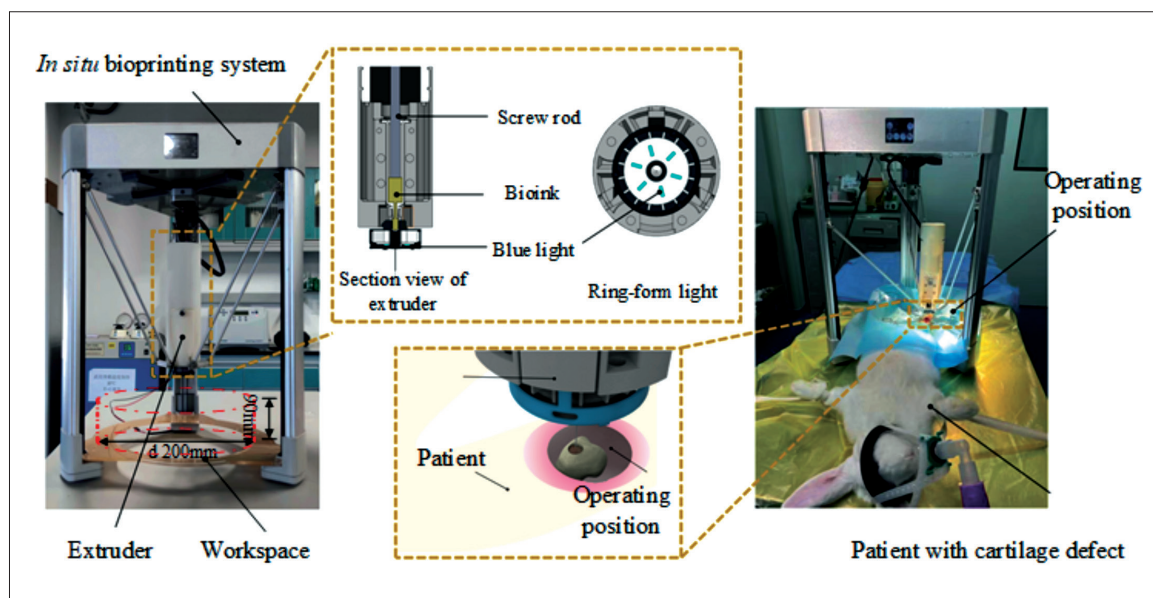
Figure 1. Schematic diagram of in situ bioprinting.

like configuration to produce light in a circular pattern. The ring-like light can prevent the hydrogel near the needles from early curing, which would, if not prevented, block the needle, thereby decreasing the printing efficiency and accuracy.

2.2. Optimization of printing parameters
To optimize the printing parameters of the parallel manipulator, Simplify3D software (USA) was used to slice a block with dimensions of 10 mm× 10 mm× 2 mm to layers with a thickness of 0.15 mm. The infill pattern was rectilinear, and the distance between lines was set at 0.5 mm. By adjusting the speed rate and extrusion multiplier, different types of scaffolds were obtained under different parameters, and their morphology was observed under a microscope.

2.3. Biocompatibility of 3D-printed scaffold
The bioink used in this study was a cartilage repair ink (TM GMP, SinoBioPrint, China), which consists of gelatin methacrylate (GelMA), chondroitin sulfate methacrylate (CSMA), and HAMA.

First, the toxicity of the 3D-printed scaffold was evaluated. A suspension of bone marrow-derived mesenchymal stem cells (BMSCs; 2×10^4 mL^{-1}) of a rabbit in exuberant growth was prepared, and 100 μL of the suspension was seeded in a 96-well plate. After culturing in an incubator for 12 h, 10 μL of scaffold leach liquor or phosphate-buffered saline (PBS) was added to each well. After incubation for 12 h, 24 h, and 48 h, the original medium in the well was replaced with 10 μL cell counting

kit-8 (CCK-8) solution and 100 μL culture medium. After incubation for 1 h, 110 μL of the liquid was removed from each well and placed into a new 96-well plate, and the absorbance values were read using a microplate reader (Thermo, Waltham, USA). The cell viability was determined using Equation I:

$$Cell\,viability(\%) = \frac{As - Ab}{Ac - Ab} \times 100 \qquad (1)$$

where As, Ac, and Ab are the optical density (OD) values of leach liquor of scaffolds, PBS, and blank, respectively.

For the cell proliferation and distribution evaluation, 200 μL of cell suspension (5×10^5 mL^{-1}) was seeded on the scaffold, and CCK-8 and Live/Dead assays were conducted to assess the relevant indicators of the cells in scaffolds; more details can be found in our previous work.[33]

2.4. Defect segmentation and reconstruction
To recognize the defect, a camera was used to capture images of the defect, and machine vision was applied to process the images. A checkerboard was placed on the defect to calibrate the camera using the machine vision toolbox of MATLAB (MathWorks, USA).[34] The *detectCheckerboardPoints* function was used to obtain the information of the checkerboard points. Four points were selected to be compared with the actual corresponding points to determine the relationship between the image coordinates and the actual ones. By applying this affine relationship, the image of the defect was converted. Through grayscale conversion, frequency statistics, and bimodal

method, the defect could be segmented from the image. By further applying the MATLAB isosurface function, the pixels in the 2D image were linked into triangular facets, and a 3D model of the defect was ultimately generated.

2.5. *In vivo* experiment

Fifteen adult New Zealand rabbits, weighing 3.5 kg each, were used in the *in vivo* experiments and randomly divided into three groups: blank group, direct implantation group, and *in situ* bioprinting group. First, a lateral parapatellar incision was made on the articular surface, and a chondral defect with a length of 2 mm and a diameter of 5 mm was made at the center of the trochlear groove. In the direct implantation group, the cartilage repair ink was cured into a cylinder by 405-nm light and then implanted into the defect. The blank group was left untreated. With regard to the *in situ* bioprinting group, the defect was repaired by the parallel manipulator. The detailed surgical procedure is exhibited in Figure 2. After the defect was identified, the image information of the defect was obtained. Subsequently, a checkerboard was placed above the defect. Through the checkerboard, the relationship between image pixel distance and actual distance was determined. Next, defect reconstruction and path planning were performed based on the checkerboard and the cartilage defect image. Finally, *in situ* bioprinting was performed. After completing the corresponding treatment in the different groups, joint reduction was performed, and the incision was closed in a layer-by-layer manner. After the disinfection of the incision area with 75% alcohol, all rabbits were moved into their cages. Within 3 days after surgery, penicillin sodium (100,000 U/kg) was injected intramuscularly. All rabbits were allowed to move freely. At 12 weeks after surgery, they were subjected to batch killing. Imaging examination, gross observation, and histological analysis were conducted, and the details can be found in the Supplementary File.

All the animal experiment protocols were approved by the Ethical Committee of Laboratory Animals of Peking University Third Medical School and were conducted in adherence with the Guide for the Care and Use of Laboratory Animals (A2022008).

2.6. Statistical analysis

All experiments were repeated at least four times, and the results are expressed as mean ± standard deviation. Two-sided, non-paired *t*-test was used for statistical comparison, and the statistical significance was set at $P < 0.05$.

3. Results

3.1. Results of printing parameter optimization

The bioprinting process was optimized by adjusting the feed rate and printing speed. Figure 3 illustrates the optimization results of the printing parameters, where the red area denotes that effective extrusion could not be achieved, the yellow area indicates that the feeding of materials was insufficient, the blue area indicates that the filament diameter was too thick, the orange area means that adjacent filament strands were stuck together, and the green area indicates that the extrusion was appropriate. In general, a high ratio of feed rate to printing speed triggers excessive feed of bioink, which results in an oversized filament. Such an oversized filament may stick to the adjacent filament, leading to a smaller hole. In the case of low ratio, the supplement of the filament will become insufficient, making the filament in the scaffold discontinuous. In this study, under a low extrusion multiplier (<0.08), when the printing speed was high, the material failed to extrude; at lower speeds, a scaffold could be formed but with a discontinuous filament. Under a high extrusion multiplier, the adjacent filaments were stuck together irrespective of the speed. Under a medium extrusion multiplier, the diameter of the filament printed at low speed was too large compared to the scaffold printed at high speed. According to the results, the appropriate printing parameters were 400–560 mm/min with an extrusion multiplier of 0.09–0.1.
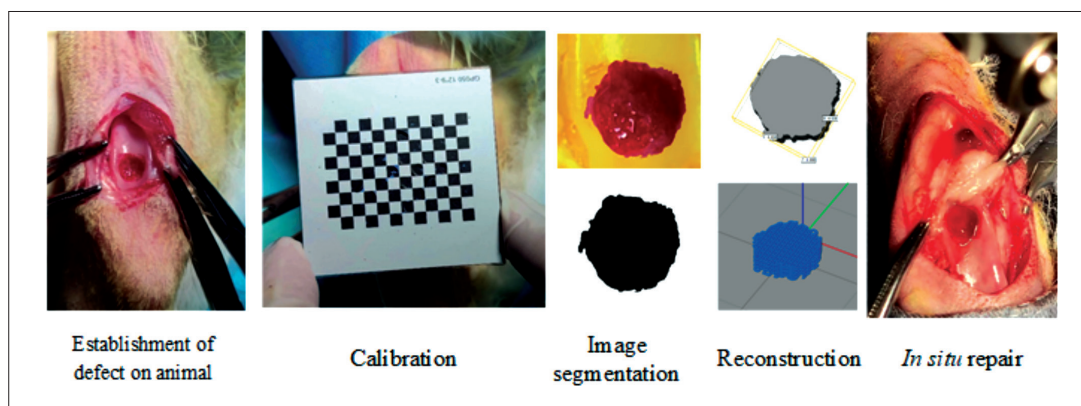

Figure 2. *In situ* 3D bioprinting process.

Figure 3. Printing parameter optimization result. The colors in the table denote different results; red: fail to form; yellow: the filament is discontinuous; blue: the filament diameter is too thick; orange: the filaments stic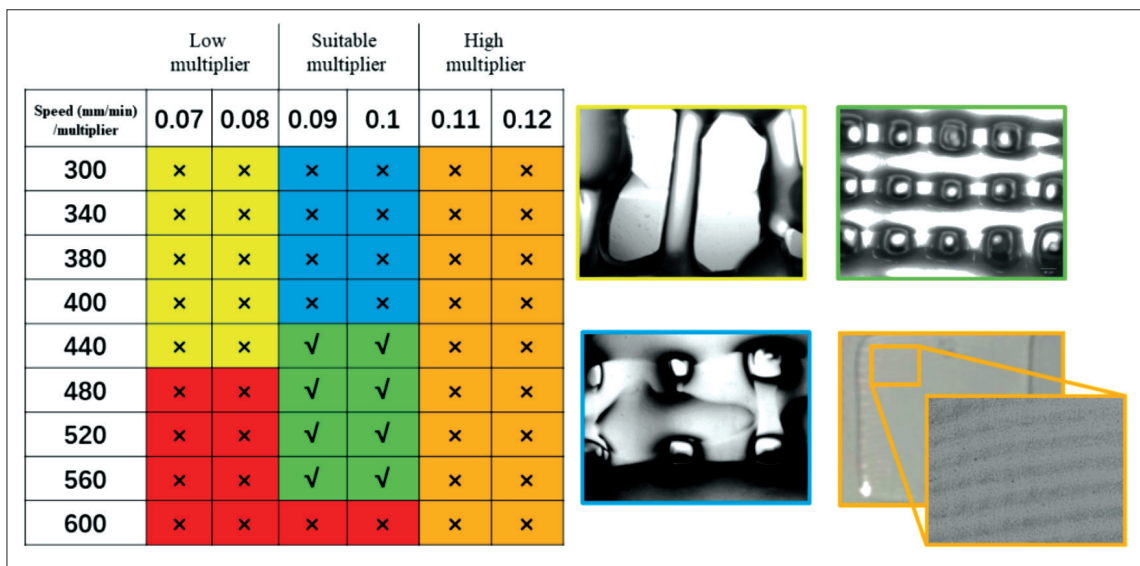k together; green: the extrusion is appropriate. Figure 3. Printing parameter optimization result. The colors in the table denote different results; red: fail to form; yellow: the filament is discontinuous; blue: the filament diameter is too thick; orange: the filaments stick together; green: the extrusion is appropriate.

3.2. Image segmentation and reconstruction

The bimodal method is a means of segmentation of images with simple background. In this study, we used bimodal method to divide images based on the regular distribution of grayscale values in the image histogram. With a simple background, the target and background appear as two clearly discernible peaks in the histogram; thus, the valley between two peaks can be selected as the threshold for image segmentation. Figure 4 depicts the image segmentation procedure. First, the image of the defect is obtained and calibrated based on affine transformation (Figure 4a). Subsequently, the color image is converted into grayscale (Figure 4b). By identifying the frequency distribution of the different grayscale values in the image, the histogram of the grayscale distribution can be obtained (Figure 4c). By setting the value of the valley between the two peaks as the threshold, a segmented image is obtained (Figure 4d), where the yellow region denotes the healthy cartilage (background) and the black one the defect (target). As presented in Figure 4e, by further applying image morphological processing, the small interference of the image can be removed (red circles in Figure 4d), and the final image of the defect is obtained.

After image segmentation, it is necessary to reconstruct the defect based on the acquired image. To verify the accuracy of the segmentation and reconstruction methods utilized in this research, model validation was performed; a flowchart depicting the image calibration and reconstruction process is illustrated in Figure 5. First, a fixed camera was used to photograph the checkerboard on the model. Subsequently, an affine matrix was obtained based on the relationship between the actual positions of the four corner points in the calibration board (red circles) and the corresponding pixel positions, thereby correcting the camera posture. Through further transformation, the actual image of the sample placed horizontally was obtained. According to the measured results, the error of the reconstructed model was about 2%, indicating that the bimodal and calibration methods can effectively recognize and reconstruct the defect.

3.3. Biocompatibility

As shown in Figure 6a, after *in vitro* culturing for 24 h, 48 h, and 72 h, the cell viability was above 85%, indicating that the bioink was non-toxic. Furthermore, the proliferation of cells on the scaffold was evaluated by CCK-8 assay, and the result is shown in Figure 6b. As the cultivation time elapsed, the OD value became higher, indicating that the number of cells increased. Nevertheless, the growth rate decelerated after culturing for 4 days. Meanwhile, the live/dead staining result revealed that most of the cells survived and were evenly distributed on the scaffold. Overall, the *in vitro* results confirmed non-cytotoxicity of the bioink, evidenced by the normal cell growth on the scaffold printed by the parallel manipulator.

3.4. Animal experiments

At 12 weeks after surgery, magnetic resonance imaging (MRI) examination was performed on the cartilage defect area of each specimen. The MRI results (Figure 7a) revealed that the cartilage signal in the cartilage defect
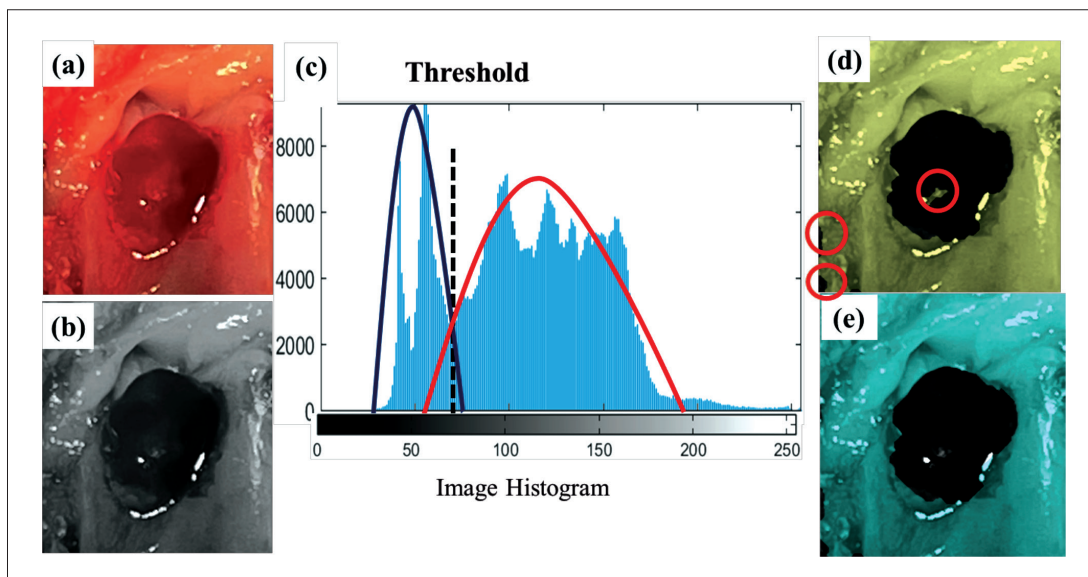
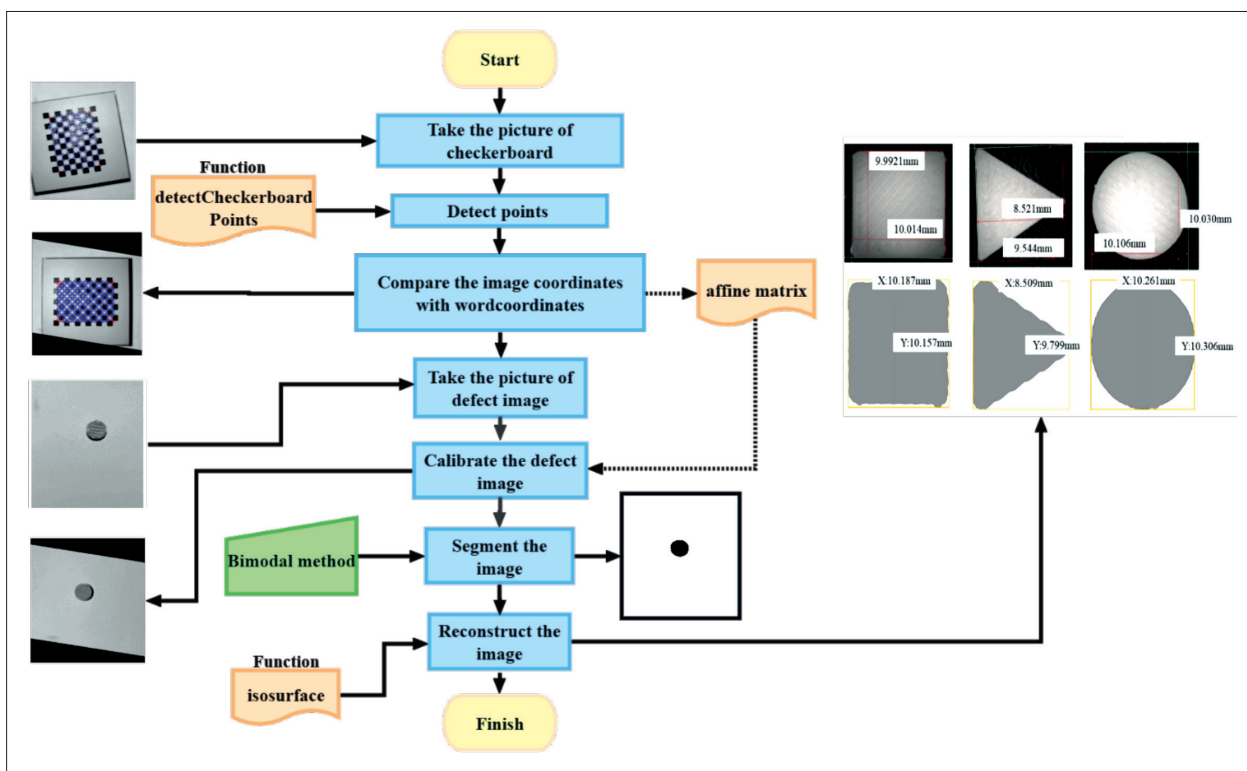**Figure 4.** Bimodal method for defect segmentation.

Figure 5. Image calibration and reconstruction process (left) and reconstruction results (right).

area of the *in situ* bioprinting group was continuous and uniform, and the fusion with the surrounding cartilage tissue was proper. With regard to the direct implantation group, an abnormal signal was detected in the subchondral bone. For the blank group, the signal of the cartilage was discontinuous. According to the MRI results, a more satisfactory regeneration result was seen in the *in situ* bioprinting group than in other groups. As shown in Figure
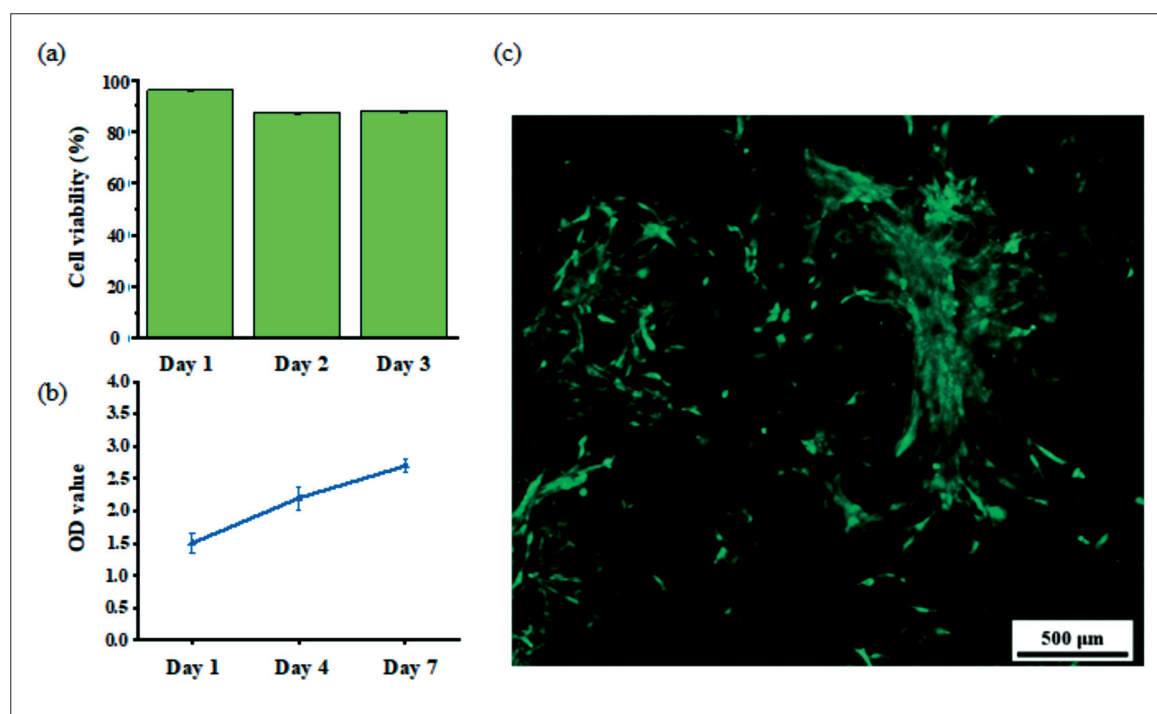
Figure 6. Results of *in vitro* experiments. (a) Cytotoxicity (n = 4). (b) Cell proliferation (n = 4). (c) Live/dead staining.

7b, in all groups, the defect was filled with regenerated tissue. However, the surface morphology of the different groups was variable. The regenerated tissues of the direct implantation and blank groups were rough compared to that of the *in situ* bioprinting group.

The histological results are presented in Figure 7c–f. According to the hematoxylin–eosin (H&E) staining results, the cells had normal morphology and grew adjacent to the healthy cartilage; however, the cells in the blank group were in disordered fashion. Furthermore, an obvious crack was found in the direct implantation group. After the Toluidine blue (TB) staining, the regenerated tissue in the blank group demonstrated light staining, which is indicative of the lesser amount of chondroid ECM compared with other groups. With regard to the *in situ* bioprinting and direct implantation groups, the staining of the repaired area was of stronger intensity. Through the Safranin O staining, it was confirmed that the major component in the regenerated tissue was glycosaminoglycan, which is a fundamental component of cartilage. Furthermore, immunohistologic staining was conducted to determine the content of type II collagen in the repair area. The staining results indicated that the fusion of the regenerated tissue in the *in situ* bioprinting group was better than that in the other groups, confirming that *in situ* bioprinting is beneficial to cartilage repair. Finally, the International Cartilage Repair Society (ICRS) and Wakitani scoring systems were

employed to evaluate the treatment efficacy shown in the different groups (Figure 7g and h). The scores of the direct implantation and *in situ* bioprinting groups were higher than those of the blank group, indicating that the hydrogel was beneficial for the cartilage. Moreover, the score of the *in situ* bioprinting group was slightly higher than that of the direct implantation group, which confirmed that *in situ* bioprinting was beneficial to cartilage repair.

4. Discussion

Bioprinting is a promising technology, through which complex organs and tissues can be fabricated in a layer-by-layer manner. After the scaffold was printed by the *in vitro* bioprinting, the preparation procedure covering processes from fabrication to surgical implantation is complicated, thus making it vulnerable to the risk of contamination. Apart from the risk of contamination, the shape of *in vitro*-printed scaffolds is fixed, hindering their ability to adapt to unexpected situations during surgery. During *in situ* bioprinting, the bioink can be deposited directly into the defect, accelerating the biomaterial delivery into the defect and diminishing the manual interventions or other adverse environmental effects.[19] In addition, the tissue near the defect can act as support during *in vivo* bioprinting, making overhanging structures printable without requiring extra supports. Moreover, the accurate deposition of the bioink can ensure that the scaffold
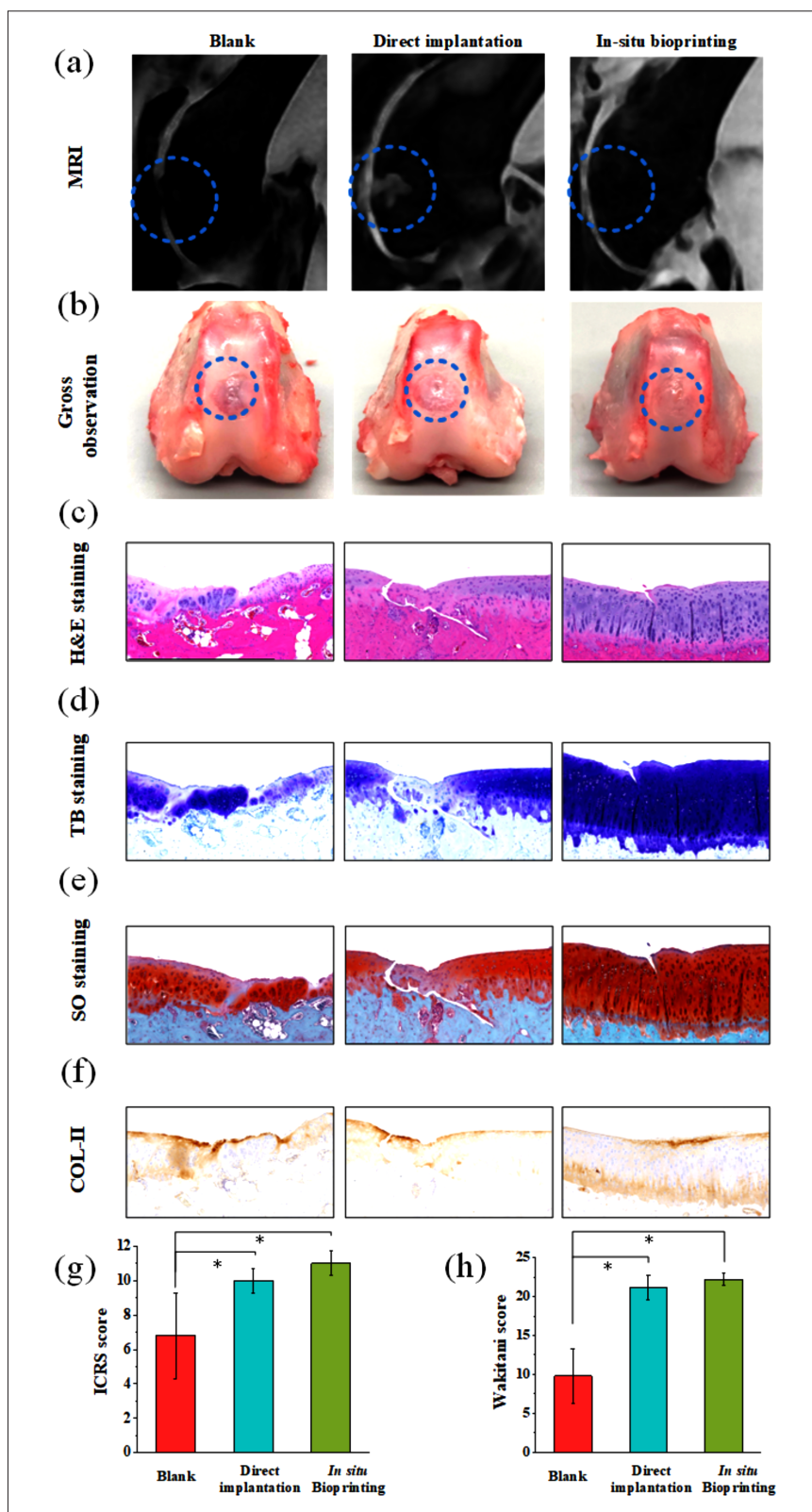
Figure 7. Results of *in vivo* experiments. (a) MRI image. (b) Gross observation. (c) H&E staining. (d) TB staining. (e) Safranin O staining. (f) Immunohistologic staining for type II collagen. (g) ICRS macroscopic evaluation of cartilage repair (n = 5). (h) Wakitani score for repaired cartilage (n = 5).

matches the defect. More importantly, due to the uncertain parameters associated with *in vitro* culturing, the *in situ* approach provides the natural microenvironment for cell growth, proliferation, and differentiation, which can promote tissue regeneration.[35,36] To this end, an *in situ* bioprinting device was developed for efficient cartilage repair.

It costs about RMB1500 to build a custom-made manipulator (details for each component can be found in the Table S1). In the articulated manipulator, the joints are connected consecutively to each other, resulting in a longer transmission chain. Without a proper control method, the long transmission chain may lead to a more severe transmission error, since the wrong movement of a joint will affect the adjacent ones. Due to the longer transmission chain, the positional accuracy of the articulated manipulator is poor.[37] Different from the articulated manipulator, the actuators in a parallel manipulator are connected directly with the base and the end effector, making it more rigid and stable.[38] Due to its high rigidity and stability, the parallel manipulator has higher accuracy and quicker responses.[39] Therefore, in order to achieve efficient *in situ* cartilage repair, a parallel manipulator was utilized in the present study.

As for the direct-writing bioprinting technology, the uniformity of the extruded filament is related not only to the rheological properties of the material, but also to the printing process.[40] On the premise that the material is printable, the printing parameters, i.e., the moving speed of the printing head and the extrusion speed of the material, have an overall impact on the quality of the printed scaffold. In this study, optimization of the aforementioned parameters was achieved by adjusting the printing speed and extrusion multiplier in the slicing software. The experiments revealed that the extrusion multiplier plays a major role in the success of printing, while the printing speed affects the quality of the printed scaffold. More specifically, when the multiplier was high, the filament accumulated together under both high and low speeds due to over-extrusion, resulting in no macroscopic pores in the scaffold. On the other hand, when the multiplier was low, the extrusion rate became low as well. At high speed, no material was extruded, resulting in forming failure; at low speed, although the material was able to flow through the needle, the extruded filament was discontinuous, which also caused invalid forming. In the case of low-speed printing and under an optimal extrusion rate, the slow movement of the printing head resulted in a longer time required for the head to travel a certain distance. Therefore, under the same extrusion rate, there was excessive extrusion material, making the filament thicker. When the printing speed was too fast, the extruded filament was pulled due to the force generated by the high-speed movement of the printing head, leading to scaffold formation failure.

The reconstruction of cartilage defects is a significant part of *in situ* bioprinting. Inspired by the traditional surgical procedure, the assessment of cartilage defects in current clinical practice is mostly based on MRI examinations, while the analysis of color images of cartilage defects is rarely performed.[41,42] In addition, there are limited corresponding image analysis methods for defects that are discovered during the operation and have never been detected in the pre-operative examinations. Due to the simple environment during surgery and the distinct color difference between healthy and injured cartilage (healthy = white; injured = red), the grayscale distribution of defects has apparent bimodal distribution characteristics. Based on the grayscale histogram, a defect can be segmented using the threshold determined by the bimodal method.

Furthermore, the biocompatibility of the printed scaffold was evaluated. The overall viability of cells in the printed scaffold was higher than 85%, and there was no statistically significant difference between the experimental and control groups, indicating that the scaffold was non-toxic for the cells. The proliferation experiment and live/dead staining results further confirmed that the printed scaffold was beneficial to cell growth and could be used in animal experiments. *In vivo* experiments were conducted to determine whether *in situ* bioprinting is beneficial to cartilage repair. In the present study, we utilized a bioink comprising HAMA, CSMA, and GelMA, which have been shown to play an important role in chondrocyte survival and phenotypic maintenance.[43,44] More specifically, hyaluronic acid is an important component of the synovial fluid, which acts as lubricant in the joint cartilage to absorb shocks.[45] Hyaluronic acid provides stimulus for chondrogenesis, promotes ECM deposition, and restrains the inflamed macrophages, thus promoting cartilage repair.[46,47] Chondroitin sulfate contributes to cartilage regeneration by diminishing inflammation, regulating metabolism, and absorbing water or nutrients.[48-51] Compared to the direct implantation group, the *in situ* bioprinting group demonstrated better fusion of the scaffold with the surrounding cartilage. This may have resulted from the shape mismatch between implantation site and implanted scaffold.[25] The matching degree of the implanted scaffold has a significant effect on the success of the surgery.[13,36] In particular, the defect was not as round as the preformed scaffold. Due to this mismatching, a void existed in the direct implantation group after implantation. The existence of the void resulted in local instability, looseness, and detachment of the scaffold, which were not conducive to tissue regeneration.[52,53] Consequently, the regeneration in the direct implantation group was not as

good as that in the *in situ* bioprinting group. Nevertheless, due to the limited research on the *in situ* bioprinting for cartilage repair, the mechanisms of *in situ* bioprinting in repairing cartilage defects remain to be delineated, and thus, more investigations are warranted.[24]

5. Conclusion

In this paper, *in situ* repair of cartilage defects was achieved using a parallel manipulator. Accurate control of the filament diameter during printing can be achieved through process optimization. The bimodal method was conducted for the defect segmentation, and a self-compiled code was developed to perform *in situ* reconstruction of the defects. The *in vitro* and *in vivo* experiment results showed that *in situ* bioprinting for the purposes of repairing cartilage defects can be realized with *in situ* 3D printing technology, which shows promising potential in clinical applications. In practice, there may be certain differences in the *z*-axis of cartilage defects. In this study, only one camera was used to capture images of the defect, and thus only planar information was retained. To remedy this shortcoming, depth camera should be utilized in future work to further optimize the 3D information.

Conflict of interest

The authors declare that they have no known competing financial interests or personal relationships that could have appeared to influence the work reported in this paper.

Author contributions

Conceptualization: Jia-Kuo Yu, Chang-Hui Song
Formal analysis: Hao-Yang Lei, You-Rong Chen, Zi-Bin Liu, Yi-Nong Li
Investigation: Hao-Yang Lei, You-Rong Chen, Bing-Bing Xu
Methodology: Hao-Yang Lei, You-Rong Chen, Bing-Bing Xu
Project administration: Jia-Kuo Yu
Writing – original draft: Hao-Yang Lei
Writing – review & editing: Hao-Yang Lei, You-Rong Chen, Bing-Bing Xu

Ethics approval and consent to participate

All the animal experiment protocols were approved by the Ethical Committee of Laboratory Animals of Peking University Third Medical School and were conducted in adherence with the Guide for the Care and Use of Laboratory Animals (A2022008).

Consent for publication

Not applicable.

Availability of data

Data used in this work is available from the corresponding author upon reasonable request.

References

1. Li M, Yin H, Yan Z, et al. The immune microenvironment in cartilage injury and repair. *Acta Biomater*. 2022;140:23-42.
   doi: 10.1016/j.actbio.2021.12.006

2. Guo X, Ma Y, Min Y, et al. Progress and prospect of technical and regulatory challenges on tissue-engineered cartilage as therapeutic combination product. *Bioact Mater*. 2023;20:501-518.
   doi: 10.1016/j.bioactmat.2022.06.015

3. Wei W, Dai H. Articular cartilage and osteochondral tissue engineering techniques: Recent advances and challenges. *Bioact Mater*. 2021;6(12):4830-4855.
   doi: 10.1016/j.bioactmat.2021.05.011

4. Chen YR, Yan X, Yuan FZ, et al. Kartogenin-conjugated double-network hydrogel combined with stem cell transplantation and tracing for cartilage repair. *Adv Sci (Weinh)*. 2022;9(35):e2105571.
   doi: 10.1002/advs.202105571

5. Zhang Y, Liu X, Zeng L, et al. Polymer fiber scaffolds for bone and cartilage tissue engineering. *Adv Funct Mater*. 2019;29(36):1903279.
   doi: 10.1002/adfm.201903279

6. Browe D, Burdis R, Diaz-Payno PJ, et al. Promoting endogenous articular cartilage regeneration using extracellular matrix scaffolds. *Mater Today Bio*. 2022;16:100343.
   doi: 10.1016/j.mtbio.2022.100343

7. Li X, Zheng F, Wang X, et al. Biomaterial inks for extrusion-based 3D bioprinting: Property, classification, modification, and selection. *Int J Bioprint*. 2022;9(2).
   doi: 10.18063/ijb.v9i2.649

8. Sadeghianmaryan A, Naghieh S, Yazdanpanah Z, et al. Fabrication of chitosan/alginate/hydroxyapatite hybrid scaffolds using 3D printing and impregnating techniques for potential cartilage regeneration. *Int J Biol Macromol*. 2022;204:62-75.
   doi: 10.1016/j.ijbiomac.2022.01.201

9. Sang S, Mao X, Cao Y, et al. 3D Bioprinting using synovium-derived MSC-laden photo-cross-linked ECM bioink for cartilage regeneration. *ACS Appl Mater Interfaces*. 2023;15(7):8895-8913.
doi: 10.1021/acsami.2c19058

10. Costa J, Silva-Correia J, Pina S, et al. Indirect printing of hierarchical patient-specific scaffolds for meniscus tissue engineering. *Bio-Des Manuf*. 2019;2(4):225-241.
doi: 10.1007/s42242-019-00050-x

11. Zou Q, Grottkau BE, He Z, et al. Biofabrication of valentine-shaped heart with a composite hydrogel and sacrificial material. *Mater Sci Eng C Mater Biol Appl*. 2020;108:110205.
doi: 10.1016/j.msec.2019.110205

12. MacAdam A, Chaudry E, McTiernan CD, Cortes D, Suuronen EJ, Alarcon EI. Development of in situ bioprinting: A mini review. *Front Bioeng Biotechnol*. 2022;10:940896.
doi: 10.3389/fbioe.2022.940896

13. Mahmoudi Z, Sedighi M, Jafari A, et al. In situ 3D bioprinting: A promising technique in advanced biofabrication strategies. *Bioprinting*. 2023;e00260.
doi: 10.1016/j.bprint.2023.e00260

14. Zhao W, Hu C, Xu T. In vivo bioprinting: Broadening the therapeutic horizon for tissue injuries. *Bioact Mater*. 2023;25:201-222.
doi: 10.1016/j.bioactmat.2023.01.018

15. Li L, Yu F, Shi J, et al. *In situ* repair of bone and cartilage defects using 3D scanning and 3D printing. *Sci Rep*. 2017;7(1):9416.
doi: 10.1038/s41598-017-10060-3

16. O'Connell CD, Di Bella C, Thompson F, et al. Development of the Biopen: A handheld device for surgical printing of adipose stem cells at a chondral wound site. *Biofabrication*. 2016;8(1):015019.
doi: 10.1088/1758-5090/8/1/015019

17. Hakimi N, Cheng R, Leng L, et al. Handheld skin printer: In situ formation of planar biomaterials and tissues. *Lab Chip*. 2018;18(10):1440-1451.
doi: 10.1039/c7lc01236e

18. Chen H, Ma X, Gao T, Zhao W, Xu T, Liu Z. Robot-assisted in situ bioprinting of gelatin methacrylate hydrogels with stem cells induces hair follicle-inclusive skin regeneration. *Biomed Pharmacother*. 2023;158:114140.
doi: 10.1016/j.biopha.2022.114140

19. Moncal K, Gudapati H, Godzik P, et al. Intra-operative bioprinting of hard, soft, and hard/soft composite tissues for craniomaxillofacial reconstruction. *Adv Funct. Mater*. 2021;31(29).
doi: 10.1002/adfm.202010858

20. Ozbolat IT, Chen H, Yu Y. Development of 'multi-arm bioprinter' for hybrid biofabrication of tissue engineering constructs. *Rob Comput Integr Manuf*. 2014;30(3):295-304.
doi: 10.1016/j.rcim.2013.10.005

21. Moncal KK, Yeo M, Celik N, et al. Comparison of *in-situ* versus *ex-situ* delivery of polyethylenimine-BMP-2 polyplexes for rat calvarial defect repair via intraoperative bioprinting. *Biofabrication*. 2022;15(1).
doi: 10.1088/1758-5090/ac9f70

22. Di Bella C, Duchi S, O'Connell CD, et al. *In situ* handheld three-dimensional bioprinting for cartilage regeneration. *J Tissue Eng Regen Med*. 2018;12(3):611-621.
doi: 10.1002/term.2476

23. Ma K, Zhao T, Yang L, et al. Application of robotic-assisted in situ 3D printing in cartilage regeneration with HAMA hydrogel: An in vivo study. *J Adv Res*. 2020;23: 123-132.
doi: 10.1016/j.jare.2020.01.010

24. Wang Y, Pereira RF, Peach C, Huang B, Vyas C, Bartolo P. Robotic in situ bioprinting for cartilage tissue engineering. *Int J Extreme Manuf*. 2023;5(3).
doi: 10.1016/j.jare.2020.01.010

25. Li L, Shi J, Ma K, et al. Robotic in situ 3D bio-printing technology for repairing large segmental bone defects. *J Adv Res*. 2021;30:75-84.
doi: 10.1016/j.jare.2020.11.011

26. Gholami P, Ahmadi-Pajouh MA, Abolftahi N, et al. Segmentation and measurement of chronic wounds for bioprinting. *IEEE J Biomed Health Inform*. 2018;22(4): 1269-1277.
doi: 10.1109/jbhi.2017.2743526

27. Lankton S, Tannenbaum A. Localizing region-based active contours. *IEEE Trans Image Process*. 2008;17(11):2029-2039.
doi: 10.1109/TIP.2008.2004611

28. Yu Y, Wang C, Fu Q, et al. Techniques and challenges of image segmentation: A review. *Electronics*. 2023;12(5).
doi: 10.3390/electronics12051199

29. Dexter A, Race AM, Steven RT, et al. Two-phase and graph-based clustering methods for accurate and efficient segmentation of large mass spectrometry images. *Anal Chem*. 2017;89(21):11293-11300.
doi: 10.1021/acs.analchem.7b01758

30. Shi H, Lee W. Image segmentation using K-means clustering, Gabor filter and moving mesh method. *Imaging Sci J*. 2023; 69(5-8):407-416.
doi: 10.1080/13682199.2022.2161159

31. Zhang F, Sun Z, Song M, Lang X. Progressive 3D shape segmentation using online learning. *Comput Aided Design*. 2015;58:2-12.
doi: 10.1016/j.cad.2014.08.008

32. Niri R, Gutierrez E, Douzi H, et al. Multi-view data augmentation to improve wound segmentation on 3D surface model by deep learning. *IEEE Access*. 2021;9: 157628-157638.
doi: 10.1109/ACCESS.2021.3130784

33. Lei H, Song C, Liu Z, et al. Rational design and additive manufacturing of alumina-based lattice structures for bone implant. *Mater Design*. 2022;221.
doi: 10.1016/j.matdes.2022.111003

34. Mathworks, Computer Vision Toolbox, https://ww2.mathworks.cn/help/vision/index

35. Murdock M, Badylak S. Biomaterials-based in situ tissue engineering. *Curr Opin Biomed Eng*. 2017;1:4-7.
doi: 10.1016%2Fj.cobme.2017.01.001

36. Singh S, Choudhury D, Yu F, Mironov V, Naing MW. In situ bioprinting - Bioprinting from benchside to bedside? *Acta Biomater*. 2020;101:14-25.
doi: 10.1016/j.actbio.2019.08.045

37. Richter F, Lu J, Orosco RK, Yip MC. Robotic tool tracking under partially visible kinematic chain: A unified approach. *IEEE Trans Rob*. 2022;38(3):1653-1670.
doi: 10.48550/arXiv.2102.06235

38. Feng L, Zhang W, Gong Z, Lin G, Liang D. Developments of delta-like parallel manipulators - A review. *Robot (China)*. 2014; 36(3):375-384.
doi: 10.5772/61744

39. Dong H, Hu B, Zhang W, et al. Robotic-assisted automated in situ bioprinting. *Int J Bioprint*. 2023;9(1):629.
doi: 10.18063%2Fijb.v9i1.629

40. Gao Q, Niu X, Shao L, et al. 3D printing of complex GelMA-based scaffolds with nanoclay. *Biofabrication*. 2019;11(3):035006.
doi: 10.1088/1758-5090/ab0cf6

41. Fritz R, Chaudhari A, Boutin R. Preoperative MRI of articular cartilage in the knee: A practical approach. *J Knee Surg*. 2020;33(11):1088-1099.
doi: 10.1055/s-0040-1716719

42. Potter H, Black B, Chong le R. New techniques in articular cartilage imaging. *Clin Sports Med*. 2009;28(1):77-94.
doi: 10.4103%2F0971-3026.137028

43. Chen X, Jiang C, Wang T, Zhu T, Li X, Huang J. Hyaluronic acid-based biphasic scaffold with layer-specific induction capacity for osteochondral defect regeneration. *Mater Des*. 2022;216.
doi: 10.1016/j.matdes.2022.110550

44. Schuurmans C, Mihajlovic M, Hiemstra C, Ito K, Hennink WE, Vermonden T. Hyaluronic acid and chondroitin sulfate (meth)acrylate-based hydrogels for tissue engineering: Synthesis, characteristics and pre-clinical evaluation. *Biomaterials*. 2021;268:120602.
doi: 10.1016/j.biomaterials.2020.120602

45. Agarwal G, Agiwa S, Srivastava A. Hyaluronic acid containing scaffolds ameliorate stem cell function for tissue repair and regeneration. *Int J Biol Macromol*. 2020; 165(Pt A):388-401.
doi: 10.1016/j.ijbiomac.2020.09.107

46. Amann E, Wolff P, Breel E, van Griensven M, Balmayor ER. Hyaluronic acid facilitates chondrogenesis and matrix deposition of human adipose derived mesenchymal stem cells and human chondrocytes co-cultures. *Acta Biomater*. 2017;52:130-144.
doi: 10.1016/j.ijbiomac.2020.09.107

47. da Silva LP, Santos T, Rodrigues D, et al. Stem cell-containing hyaluronic acid-based spongy hydrogels for integrated diabetic wound healing. *J Invest Dermatol*. 2017;137(7):1541-1551.
doi: 10.1016/j.jid.2017.02.976

48. Agrawal P, Pramanik K, Vishwanath V, et al. Enhanced chondrogenesis of mesenchymal stem cells over silk fibroin/chitosan-chondroitin sulfate three dimensional scaffold in dynamic culture condition. *J Biomed Mater Res B Appl Biomater*. 2018;106(7):2576-2587.
doi: 10.1002/jbm.b.34074

49. Lafuente-Merchan M, Ruiz-Alonso S, Zabala A, et al. Chondroitin and dermatan sulfate bioinks for 3D bioprinting and cartilage regeneration. *Macromol Biosci*. 2022;22(3):e2100435.
doi: 10.1002/mabi.202100435

50. Tan G, Tabata Y. Chondroitin-6-sulfate attenuates inflammatory responses in murine macrophages via suppression of NF-kappaB nuclear translocation. *Acta Biomater*. 2014;10(6):2684-2692.
doi: 10.1016/j.actbio.2014.02.025

51. Wang D, Varghese S, Sharma B, et al. Multifunctional chondroitin sulphate for cartilage tissue-biomaterial integration. *Nat Mater*. 2007;6(5):385-392.
doi: 10.1038/nmat1890

52. Kwon H, Brown W, Lee C, et al. Surgical and tissue engineering strategies for articular cartilage and meniscus repair. *Nat Rev Rheumatol*. 2019;15(9):550-570.
doi: 10.1038%2Fs41584-019-0255-1

53. Trengove A, Di Bella C, O'Connor A. The challenge of cartilage integration: Understanding a major barrier to chondral repair. *Tissue Eng Part B Rev*. 2022;28(1):114-128.
doi: 10.1089/ten.teb.2020.0244